

Ultrafast resonant optical scattering from single gold nanorods: Large nonlinearities and plasmon saturation

Matthew Pelton,* Mingzhao Liu, Sungnam Park,† Norbert F. Scherer, and Philippe Guyot-Sionnest
*Department of Physics, Department of Chemistry, and James Franck Institute,
University of Chicago, 5640 S. Ellis Ave., Chicago, IL 60637*

(Dated: May 1, 2019)

We measure nonlinear optical scattering from individual Au nanorods excited by ultrafast laser pulses on resonance with their longitudinal plasmon mode. Isolating single rods removes inhomogeneous broadening and allows the measurement of a large nonlinearity, much greater than that of nanorod ensembles. Surprisingly, the ultrafast nonlinearity can be attributed entirely to heating of conduction electrons and does not exhibit any response associated with coherent plasmon oscillation. This indicates a previously unobserved damping of strongly driven plasmons.

PACS numbers: 78.67.Bf, 78.47.+p

I. INTRODUCTION

Conventional photonic devices are restricted by the diffraction limit to be larger than half the optical wavelength, limiting the possibilities for miniaturization.¹ One way to overcome this limit is to couple light to material excitations. Of particular interest are collective electron oscillations in metal nanostructures, termed surface plasmons.^{2,3} Plasmons allow for nanoscale delocalization, transport of electromagnetic energy, and large local field enhancements. Preliminary steps have been made, for example, towards using surface plasmons in nanoparticles to construct sub-wavelength waveguides.^{4,5} Actively controlling light propagation in such structures will require an understanding of the ultrafast nonlinear response of the individual elements. Such an understanding is also crucial for the treatment of effects such as surface-enhanced Raman scattering,^{6,7} since it may limit the magnitude of local electromagnetic fields that can be achieved in real structures.

Previous measurements of metal-nanoparticle nonlinearities have generally involved excitation at frequencies away from the plasmon resonance, and thus probe incoherent effects related to the heating of electrons.^{8,9,10,11,12,13,14} Exciting and probing nanoparticles on resonance with their plasmon frequencies can reveal nonlinearities associated with the coherent oscillation of the plasmons themselves. Unfortunately, the optical response of the ensemble is broadened by the inhomogeneous distribution of particle sizes and shapes. The majority of particles are off resonance with the exciting laser, and thus have nonlinear responses much smaller than or even opposite in sign to the resonant particles. This leads to an overall measured effect that is greatly reduced and whose dynamics are obscured. By contrast, isolating single particles allows the quantitative measurement of inherent properties.^{15,16,17}

We report the first measurements of resonant nonlinearities of surface plasmons in single metal nanoparticles, specifically Au nanorods.^{18,19} We measure a nonlinear scattering cross-section that is much larger than that

obtained from ensembles of nanorods. Surprisingly, the measured effect can be explained entirely as the result of heating of conduction electrons, with no measurably nonlinearity directly associated with coherent plasmon oscillation. This indicates that the strong optical driving fields induce a novel damping and saturation of the plasmonic response.

II. EXPERIMENTAL

The Au nanorods we study are chemically synthesized using a seed-mediated growth method.^{20,21} Under the proper growth conditions, this process produces single-crystal rods with smooth surfaces, controllable aspect ratios, and > 95% yield.²² A transmission-electron-microscope image of a typical nanorod is shown in Fig. 1(c). The rods exhibit a strong longitudinal plasmon resonance, whose frequency is determined by the aspect ratio of the rods.²³ Damping due to interband transitions is reduced by selecting particles with a plasmon resonance near 1.55 eV,²⁴ which matches the Ti:Sapphire laser light used to excite and probe the rods.

The gold-nanorod solution is prepared as follows. Spherical seed particles are produced by mixing 0.25 mL of 10 mM HAuCl₄ solution with 10 mL of 0.1 M CTAB (cetyltrimethylammoniumbromide) solution at room temperature, and then quickly injecting 0.6 mL of freshly prepared 10 mM NaBH₄ solution under vigorous stirring. In order to grow the seeds into rods, 50 mL of 0.1 M CTAB solution is prepared and maintained at 28 °C. To this solution, 2.5 mL of 10 mM HAuCl₄, and 0.5 mL of 10 mM AgNO₃ are added. 1.0 mL of 1.0 M HCl is also added, to maintain the stability of the final produce. Au(III) is reduced to Au(I) by injecting 0.4 mL of 0.1 M ascorbic acid. Finally, 0.12 mL of the gold-seed solution is added to begin the nanorod growth, and growth is completed overnight under steady stirring. No further size selection is performed.

The sample consists of sparsely dispersed and isolated rods, bound to a glass coverslip. The coverslip is first cleaned for 10 minutes with an equal mixture of

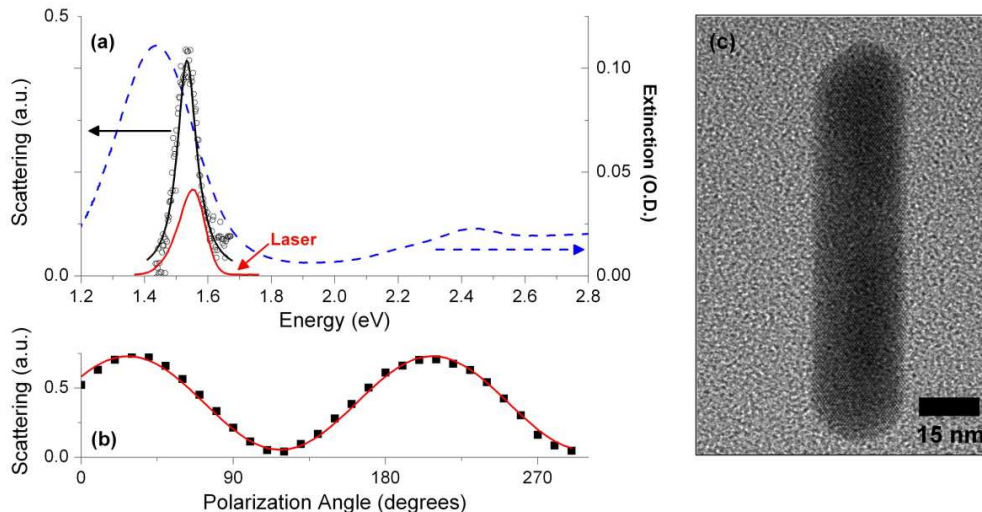


FIG. 1: (Color online) (a) Extinction of an ensemble of Au nanorods in aqueous solution (dashed blue line); scattering spectrum from a single nanorod on a glass surface (circles); calculated scattering spectrum for a single rod (solid black line); and measured spectrum of the laser used to excite the rods (solid red line). (b) Intensity of laser light scattered off a single rod as the incident laser polarization is varied (squares), and sinusoidal fit (red line). (c) Au nanorod, on a carbon grid, imaged with a transmission-electron microscope (TEM).

30% H_2O_2 and 98% H_2SO_4 , and then coated with an MPTMS (3-mercaptopropyltrimethylsilane) monolayer, using a two-step gas-phase silanization procedure.²⁵ The functionalized glass substrate is dipped into the Au-nanorod solution for 30 minutes. The sample is then washed thoroughly in deionized water and dried in air. Atomic-force microscopy (AFM) is used to verify that the rods are well isolated on the surface, so that individual rods can subsequently be probed optically.

Optical measurements on the single rods are made using total-internal-reflection microscopy.^{21,22,26} Incident light is focussed onto the sample through a glass prism. Scattered light is collected using a microscope objective and is imaged onto a multimode optical fiber, which selects a $1.5 \mu\text{m}$ spot on the sample for observation. For spectral measurements, the light is sent to a spectrometer equipped with a cooled CCD array detector (Andor); for time-resolved measurements, the light is sent to an avalanche photodiode (Hamamatsu).

III. IDENTIFICATION OF SINGLE RODS

Making single-rod measurements requires carefully ensuring that only one rod at a time is being probed. The primary method of identifying single rods is to excite with incoherent white light and measure the scattering spectrum; a typical spectrum is shown in Fig. 1(a). The narrow resonance, much less broad than the ensemble peak, indicates that the scattering comes from a single rod. If two or more nanorods are probed, they will have

different shapes, and thus different plasmon resonance frequencies; the measured scattering spectrum will then be broader than the single-rod spectrum.

The scattering spectrum is quantitatively compared to a calculation in the quasi-static approximation,^{21,22,23} as shown in Fig. 1(a). We treat the rod as a prolate ellipsoid, and approximate the asymmetric environment of the rod as a homogeneous, transparent medium with dielectric constant $\epsilon_m = 1.3$. For incident light polarized parallel to the long axis of the rod, the polarizability of the particle is

$$\alpha = V \frac{\epsilon - \epsilon_m}{\epsilon_m + L(\epsilon - \epsilon_m)}, \quad (1)$$

where V is the volume of the rod, ϵ is the dielectric function of Au, and L is a geometric factor:

$$L = \frac{1 - e^2}{e^2} \left(\frac{1}{2e} \ln \frac{1 + e}{1 - e} - 1 \right), \quad (2)$$

where e is the eccentricity of the ellipsoid. The scattering cross-section is then given by

$$\sigma_{\text{scat}} = \frac{k^4}{6\pi} |\alpha|^2, \quad (3)$$

where k is the wavenumber of the incident light.

The imaginary part of the dielectric function of Au is taken to be^{27,28,29}

$$\epsilon_2(\omega, T_e) = \frac{\omega_p^2 \gamma(T_e)}{\omega [\omega_p^2 + \gamma(T_e)^2]} + \epsilon_2^{d-c}(\omega, T_e), \quad (4)$$

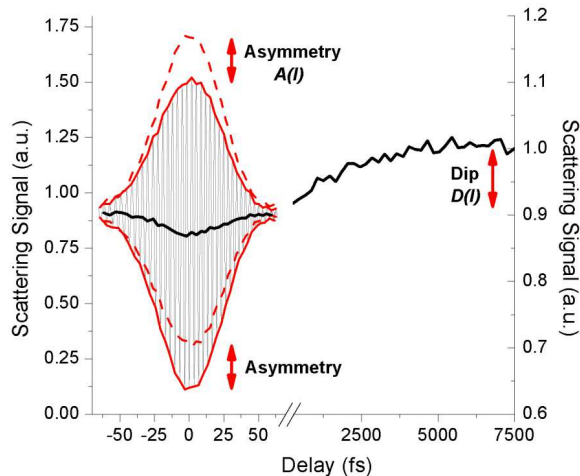


FIG. 2: (Color online) Single-rod scattering signal as a function of delay between two incident laser pulses. Left-hand side: scattering intensity for overlapping pulses with an energy of 47 pJ (light line); envelope of the interference pattern (solid red line); the same envelope, inverted about the average scattering signal at a delay of 75 fs (dashed red line); and the average of the upper and lower envelopes (heavy line). Right-hand side: scattering intensity for non-overlapping pulses with an energy of 94 pJ. Note that both vertical and horizontal scales are different on the two sides of the graph.

where ω is the optical frequency and T_e is the temperature of the conduction electrons in the rod. The first term is the Drude free-electron contribution; ω_p is the bulk plasmon frequency, and γ is the plasmon damping rate. The second term is the contribution of transitions between the d and the conduction bands. The real part of the dielectric function is calculated from this imaginary part using the Kramers-Kronig relation. The matrix elements of the interband transitions and the Drude plasmon frequency are adjusted to reproduce experimental dielectric functions.³⁰

In comparing the calculated and measured scattering spectra, the only free parameter is the aspect ratio of the rod. For the particular rod in Fig. 1(a), the fitted aspect ratio is 5.25, consistent with the rod shapes measured by TEM. A different choice of refractive index for the surrounding medium changes the fitted nanorod aspect ratio, but has no other appreciable effect on calculated optical properties. The very good agreement between the calculated and measured scattering linewidths is thus a clear indication that only a single rod is being probed.

Identification of single rods is further supported by the strong polarization dependence of the scattering, as shown in Fig. 1(b). The nearly complete modulation is consistent with scattering from a single, oriented dipole, rather than multiple particles.

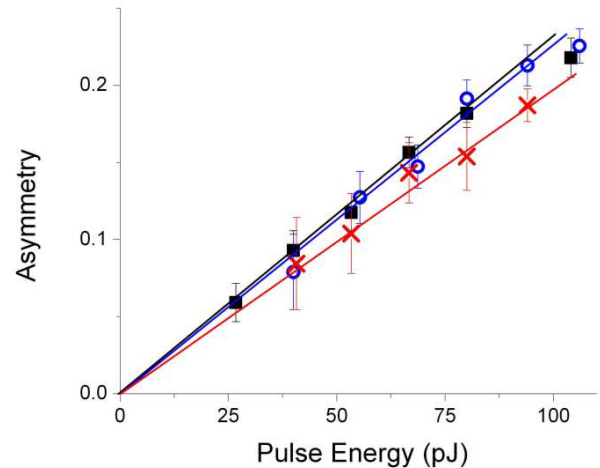


FIG. 3: (Color online) Measured asymmetry in interference patterns for three different rods.

IV. ULTRAFAST NONLINEARITIES

Nonlinearities of the single nanorods are measured using an interferometric scattering technique. The rods are excited with 20-fs pulses from a mode-locked, cavity-dumped Ti:Sapphire laser.³¹ The pulses are split into two equal-intensity parts,^{16,32} and the delay of one of the pulses is controlled relative to the other by moving a retroreflector, using either a calibrated stepper motor or a piezoelectric transducer. A single lens focuses the two pulses to a common 20- μm spot on the sample. The signal is processed by a lock-in amplifier, which is synchronized to a chopper that modulates both laser beams.

Fig. 2 shows an example of the scattering signal from a single rod for short delays; the measured interference pattern exhibits a pronounced asymmetry in intensity. When the laser pulses interfere constructively, the incident intensity is doubled, but the amount of scattering from the rod increases by less than a factor of two, meaning that the scattering cross-section of the rod is smaller for the higher intensity. The interference patterns do not change as the repetition rate of the laser is varied, indicating that slow, cumulative effects are not important. The nonlinearity thus arises within the 20-fs pulse duration.

These measurements make it possible to establish the magnitude of the ultrafast nonlinearity. Figure 3 shows for different rods the measured asymmetry as a function of the laser intensity, I , in each pulse. The nearly linear dependence indicates a third-order nonlinearity. That is, the scattering cross-section can be written $\sigma(I) = \sigma^{(0)} + I\sigma^{(3)}$, so that the measured asymmetry should be

$$A(I) = 4I \frac{\sigma^{(3)}}{\sigma^{(0)} - 2I\sigma^{(3)}}. \quad (5)$$

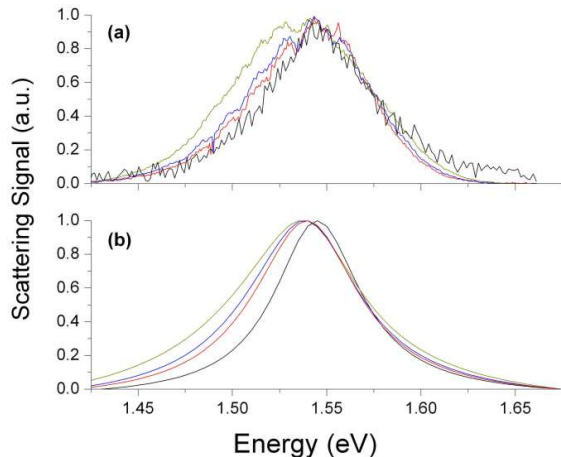


FIG. 4: (Color online) (a) Measured single-rod scattering spectra for different incident intensities. The rightmost curve is the linear spectrum measured using incoherent, broadband excitation. The other curves are measured using a single laser beam, and correspond to pulse energies of 52, 82, and 192 pJ, from right to left. The spectra are normalized for ease of comparison. (b) Corresponding calculated scattering spectra, assuming spectral changes are due to instantaneous heating of conduction electrons.

As shown in Fig. 3, this formula fits our data well.

The fit to the data gives a normalized nonlinear cross-section $\sigma^{(3)}/\sigma^{(0)} = (7.5 \pm 0.9) \times 10^{-11} \text{ cm}^2/\text{W}$. Transient-transmission measurements on nanorod ensembles in solution show a corresponding average nonlinear cross-section of approximately $2.5 \times 10^{-13} \text{ cm}^2/\text{W}$,³³ the significantly lower value is the result of the large number of non-resonant nanorods, whose nonlinearities are smaller than and can even oppose those of the resonant rods. The single-rod nonlinear cross-section also implies a nonlinear susceptibility for Au over the laser bandwidth of $\chi^{(3)} \approx 5 \times 10^{-18} \text{ m}^2/\text{V}^2$. As a result of this large nonlinearity, the change in scattering cross-section can reach over 20% at high laser intensities. If the laser power is increased further, optical damage occurs, and the scattering signal gradually and irreversibly decreases.

Further insight into the measured nonlinearity is obtained by measuring the dependence of the nanorod scattering spectrum on incident laser power. Results for a particular nanorod are shown in Fig. 4(a); an intensity-dependent red shift $\Delta\omega$ and line broadening $\Delta\gamma$ are clearly seen. Both effects are linear in I ; for this rod, $\Delta\omega = 59 \text{ meV/nJ}$, and $\Delta\gamma = 87 \text{ meV/nJ}$.

V. PICOSECOND NONLINEARITIES

Having established the magnitude of the nonlinearity, we next investigate its time dependence. To do so, we

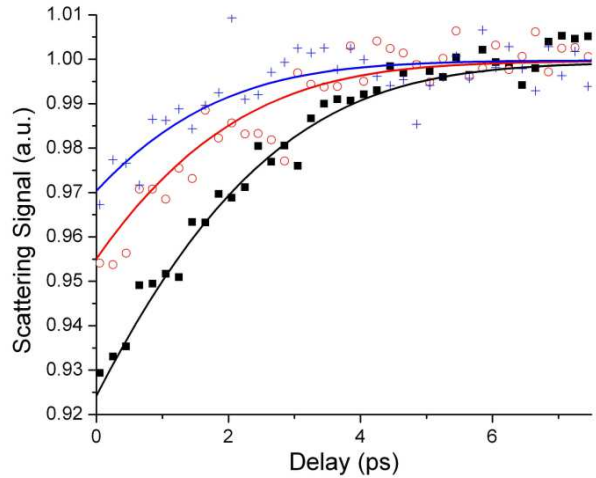


FIG. 5: (Color online) Measured single-rod scattering signal as a function of time delay between two incident laser pulses, normalized by the measured signal at a delay of 20 ps (points), and calculated change in scattering (lines). The three curves, from top to bottom, correspond to pulse energies of 26, 53, and 94 pJ.

perform measurements with longer time delays, so that the two laser pulses no longer overlap. Figure 2 shows a representative result, and Fig. 5 gives similar results for different laser powers. The response is characteristic of the heating of conduction electrons by the laser pulse, followed by their cooling and equilibration with lattice phonons.^{9,10,11,33} Increasing the delay up to 150 ps results in no detectable change in the scattering signal, indicating that effects related to the heating of lattice phonons are unimportant on experimental time scales. The data in Fig. 5 have been normalized to the signal at long delays; any ultrafast nonlinearity arising within the laser pulse duration will result in a change in this reference level, but will not otherwise affect the time-delay-dependent data.

The picosecond-scale results can be modeled as follows. The amount of light transferred from the first laser pulse to the conduction electrons is determined by calculating the nanorod absorption cross-section; this energy transfer results in a higher electron temperature, T_e . The subsequent evolution of T_e is calculated by treating the conduction electrons and the lattice phonons as two coupled thermal reservoirs.^{12,33} The time evolution of the reservoir temperatures is given by

$$C_e T_e'(t) = g [T_l(t) - T_e(t)] \quad (6)$$

$$C_l T_l'(t) = g [T_e(t) - T_l(t)], \quad (7)$$

where C_e and C_l are the heat capacities of the electrons and the lattice, respectively; T_l is the lattice temperature; and g is the electron-phonon coupling coefficient.

The effect of elevated T_e is to alter the dielectric function for Au, as described by Eqn. (4).^{27,28,29} From the dielectric function, the scattering spectrum can be calculated according to Eqns. (1) and (3). For higher electron temperatures, the plasmon is broadened and red-shifted. The modified plasmon response is used to calculate the amount of light scattered from the second laser pulse.

This calculated scattering signal is fit to the data using a single free parameter, relating the measured laser power to the optical intensity incident on the rod. Fig. 5 shows, for a single rod, results for three different laser powers. Equally good agreement was obtained for several other laser powers and for other rods, indicating that electron heating can account for the measured nonlinearity on picosecond time scales.

VI. PLASMON SATURATION

Unexpectedly, the same thermal model that explains the picosecond measurements also quantitatively explains the measured nonlinearities on femtosecond time scales. More precisely, we can extrapolate the measured thermal nonlinearity for a given laser intensity, I , to zero time delay; this gives a “dip” $D(I)$ in the normalized scattering signal. (See Fig. 2; in this case $D \approx 9\%$.) The measured values of $D(I)$ can be compared to the asymmetries, $A(I)$, of the measured interference patterns. Assuming that the only nonlinearity, even for the shortest time delays, is due to electron heating, we obtain $A(I) = 2D(2I)$. (We note that this relation takes into account the dependence of the reference level for $D(I)$ on the intensity of the two laser pulses.) We observe exactly this relation, within our experimental error, meaning that we see no change in the dynamics of the nonlinearity as we move from femtosecond to picosecond time scales.

This observation is consistent with the increase in the plasmon linewidth at high pulse energies, as shown in Fig. 3(a). Fig. 3(b) shows theoretical scattering spectra for the same pump powers, assuming that the only spectral changes are due to instantaneous heating of the conduction electrons. Differences between the calculations and the measurements, particularly in the line shapes, are likely due to femtosecond-scale dynamics that are not captured by the extreme assumption of instantaneous electron heating. Nonetheless, the good agreement provides another strong indication that a nearly thermal distribution of electrons is produced in the rod within a time short compared to the 20-fs laser pulse duration.

This is unexpected, since the resonant laser pulses should excite plasmons that remain coherent for 15 fs, based on the measured linear-scattering linewidth (see Fig. 1(a)). Any initial nonlinearity would then be due to deviation of the plasmon motion from perfect harmonic oscillation, caused, for example, by confinement of electrons by the boundaries of the rod.³⁴ The amplitude of electron oscillation can be estimated by considering the

dipole moment D induced by the applied field:

$$D = \alpha E = nde, \quad (8)$$

where E is the applied field, n is the number of electrons in the rod, d is their displacement, and e is the electronic charge. Using known material parameters for Au then gives, for pulse energies of 100 pJ, an electron displacement d approximately 8% of the rod length. The deviation from simple harmonic oscillation should then be considerable, implying a significant coherent nonlinearity. Such a mechanism would also be responsible for the generation of third-harmonic radiation by resonantly-driven plasmons.^{34,35}

The absence of any measurable coherent nonlinearity, and the immediate emergence of an incoherent thermal nonlinearity, indicate that the plasmon cannot be coherently oscillating over the duration of the laser pulse. In other words, the strong, resonant laser excitation must be responsible for increasing the plasmon damping rate and destroying its coherence. The reduction in the plasmon lifetime then means that it is impossible to resolve any coherent nonlinearities with the 20-fs pulses used.

The increased damping may be due to a greater rate of dephasing collisions with the nanorod boundaries or to higher-order plasmon-plasmon or plasmon-electron interactions. Such interactions are also manifest in the significant electron energies that are observed in photoemission measurements when plasmons are resonantly excited.^{36,37}

VII. CONCLUSIONS

The measurements described in this paper have established for the first time the magnitude of resonant optical nonlinearities in single Au nanorods. A benchmark value of 20% has been obtained for the nonlinear change in the scattering cross-section, using pulse energies that induce no optical damage. Surprisingly, resonant excitation of plasmons results in the same nonlinearity as incoherent excitation of conduction electrons. This indicates that strongly driven plasmons experience a new, intensity-dependent damping. There are still several potential routes towards achieving stronger nonlinearities in these systems, such as embedding the nanorods in a polarizable medium, or assembling them into ordered structures. Our current observations thus represent a first step towards achieving very large optical nonlinearities on the nanometer scale.

Acknowledgements

We thank Dr. A. Bakhtyari for valuable assistance and Prof. H. Petek for helpful discussions. This work was principally supported by the MRSEC program of

the NSF under grant No. DMR 0213745, with additional support from the UC-ANL Consortium for Nanoscience Research and from NSF grant No. CHE 0317009. M.P.

is supported by the Grainger Postdoctoral Fellowship in Experimental Physics from the University of Chicago.

-
- * Electronic address: pelton@uchicago.edu
 † Current address: Department of Chemistry, Stanford University, Stanford, CA 94305
- ¹ B. E. A. Saleh and M. C. Teich, *Fundamentals of Photonics* (John Wiley & Sons, New York, 1991).
 - ² W. L. Barnes, A. Dereux, and T. W. Ebbesen, *Nature* **424**, 824 (2003).
 - ³ S. A. Maier and H. A. Atwater, *J. Appl. Phys.* **98**, 011101 (2005).
 - ⁴ M. Quinten, A. Leitner, J. R. Krenn, and F. R. Aussenegg, *Opt. Lett.* **23**, 1331 (1998).
 - ⁵ S. A. Maier *et al.*, *Nature Materials* **2**, 229 (2003).
 - ⁶ S. Nie and S. R. Emory, *Science* **275**, 1102 (1997).
 - ⁷ K. Kneipp *et al.*, *Phys. Rev. Lett.* **78**, 1667 (1997).
 - ⁸ M. J. Feldstein *et al.*, *J. Am. Chem. Soc.* **119**, 6638 (1997).
 - ⁹ J. H. Hodak, A. Henglein, and G. V. Hartland, *J. Phys. Chem. B* **104**, 9954 (2000).
 - ¹⁰ C. Voisin, N. D. Fatti, D. Christofilos, and F. Vallée, *J. Phys. Chem. B* **105**, 2264 (2001).
 - ¹¹ S. Link and M. El-Sayed, *Annu. Rev. Phys. Chem.* **54**, 331 (2003).
 - ¹² A. Arbouet *et al.*, *Phys. Rev. Lett.* **90**, 177401 (2003).
 - ¹³ S. Link *et al.*, *Phys. Rev. B* **61**, 6086 (2000).
 - ¹⁴ M. Hu *et al.*, *J. Am. Chem. Soc.* **125**, 14925 (2003).
 - ¹⁵ T. Itoh, T. Asahi, and H. Masuhara, *Appl. Phys. Lett.* **79**, 1667 (2001).
 - ¹⁶ Y.-H. Liao, A. N. Unterreiner, Q. Chang, and N. F. Scherer, *J. Phys. Chem. B* **105**, 2135 (2001).
 - ¹⁷ M. A. van Dijk, M. Lippitz, and M. Orrit, *Phys. Rev. Lett.* **95**, 267406 (2005).
 - ¹⁸ M. Pelton, M. Liu, S. Park, N. F. Scherer, and P. Guyot-Sionnest, *Proc. SPIE* **5927**, 191 (2005).
 - ¹⁹ M. Pelton, M. Liu, S. Park, N. F. Scherer, and P. Guyot-Sionnest, <http://arxiv.org/abs/cond-mat/0506158>.
 - ²⁰ B. Nikoobakht and M. A. El-Sayed, *Chem. Mater.* **15**, 1957 (2003).
 - ²¹ M. Liu and P. Guyot-Sionnest, *J. Phys. Chem. B* **108**, 5882 (2004).
 - ²² M. Liu and P. Guyot-Sionnest, *J. Phys. Chem. B* **109**, 22192 (2005).
 - ²³ C. F. Bohren and D. R. Huffman, *Absorption and Scattering of Light by Small Particles* (John Wiley & Sons, New York, 1983).
 - ²⁴ C. Sönnichsen *et al.*, *Phys. Rev. Lett.* **88**, 077402 (2002).
 - ²⁵ H. Jung *at al.*, *Nano Lett.* **4**, 2171 (2004).
 - ²⁶ C. Sönnichsen *et al.*, *Appl. Phys. Lett.* **77**, 2949 (2000).
 - ²⁷ R. Rosei, F. Antonangeli, and U. M. Grassano, *Surf. Sci.* **37**, 689 (1973).
 - ²⁸ R. Rosei, *Phys. Rev. B* **10**, 474 (1974).
 - ²⁹ M. Guerrisi, R. Rosei, and P. Winsemius, *Phys. Rev. B* **12**, 557 (1975).
 - ³⁰ P. B. Johnson and R. W. Christy, *Phys. Rev. B* **6**, 4370 (1972).
 - ³¹ Y.-H. Liao, A. N. Unterreiner, D. C. Arnett, and N. F. Scherer, *Appl. Opt.* **38**, 7386 (1999).
 - ³² H. Petek and S. Ogawa, *Prog. Surf. Sci.* **56**, 239 (1998).
 - ³³ S. Park, M. Pelton, M. Liu, P. Guyot-Sionnest, and N. F. Scherer, in preparation.
 - ³⁴ M. Lippitz, M. A. van Dijk, and M. Orrit, *Nano. Lett.* **5**, 799 (2005).
 - ³⁵ B. Lamprecht, J. R. Krenn, A. Leitner, and F. R. Aussenegg, *Phys. Rev. Lett.* **83**, 4421 (1999).
 - ³⁶ G. Banfi, G. Ferrini, M. Peloi, and F. Parmigiani, *Phys. Rev. B* **67**, 035428 (2003).
 - ³⁷ A. Kubo, K. Onda, H. Petek, Z. Sun, Y. S. Jung, and H. K. Kim, *Nano Lett.* **5**, 1123 (2005).